energies

MDPI

Article

Decomposition-Based Multi-Classifier-Assisted Evolutionary Algorithm for Bi-Objective Optimal Wind Farm Energy Capture

Hongbin Zhu [2], Xiang Gao [1,*], Lei Zhao [2] and Xiaoshun Zhang [3]

[1] Industrial Training Centre, Shenzhen Polytechnic, Shenzhen 518055, China
[2] College of Engineering, Shantou University, Shantou 515063, China; 21hbzhu@stu.edu.cn (H.Z.); zhaoleichinese@163.com (L.Z.)
[3] Foshan Graduate School of Innovation, Northeastern University, Foshan 528311, China; xszhang1990@sina.cn
* Correspondence: gaoxiang@szpt.edu.cn

Abstract: With the wake effect between different wind turbines, a wind farm generally aims to achieve the maximum energy capture by implementing the optimal pitch angle and blade tip speed ratio under different wind speeds. During this process, the balance of fatigue load distribution is easily neglected because it is difficult to be considered, and, thus, a high maintenance cost results. Herein, a novel bi-objective optimal wind farm energy capture (OWFEC) is constructed via simultaneously taking the maximum power output and the balance of fatigue load distribution into account. To rapidly acquire the high-quality Pareto optimal solutions, the decomposition-based multi-classifier-assisted evolutionary algorithm is designed for the presented bi-objective OWFEC. In order to evaluate the effectiveness and performance of the proposed technique, the simulations are carried out with three different scales of wind farms, while five familiar Pareto-based meta-heuristic algorithms are introduced for performance comparison.

Keywords: wind farm; wake effect; fatigue load; Pareto-based optimization; bi-objective optimization

Citation: Zhu, H.; Gao, X.; Zhao, L.; Zhang, X. Decomposition-Based Multi-Classifier-Assisted Evolutionary Algorithm for Bi-Objective Optimal Wind Farm Energy Capture. *Energies* **2023**, *16*, 3718. https://doi.org/10.3390/en16093718

Academic Editors: Davide Astolfi, Shiwei Xia, Wei Gan, Cheng Liu, Ying Xu and Meng Song

Received: 28 March 2023
Revised: 14 April 2023
Accepted: 24 April 2023
Published: 26 April 2023

1. Introduction

In recent years, wind energy has become a major breakthrough in the development of new energy in many countries due to its clean, renewable, and environmentally-friendly features [1]. In order to save land resources and reduce investment costs, tens or even hundreds of wind turbines (WTs) are usually built into a wind farm (WF) in a certain arrangement. When the incoming wind speed passes through the upstream WTs, the wind speed for the downstream WTs decreases while the turbulence intensity increases, which is usually called the wake effect [2]. In general, the wake effect can not only reduce the power generation of the downstream WTs, but also increase the fatigue load [3] with the increasing turbulence intensity. The existing research shows that the efficiency loss of a WF influenced by the wake effect is up to 40%, and the maximum load increase can range from 10% to 45%.

To weaken the influence by the wake effect, many optimization or control methods were designed to achieve the optimal layout and operation of WTs in a wind farm. Ref. [4] explicitly incorporated the wake effect into the reliability assessment of a WF. Later, a new method for placing offshore wind turbines in regular-shaped wind farms was proposed to minimize the wake effect of wind farms [5]. Based on the consideration of wake effect, a wind farm optimal scheduling method was proposed to maximize the output power [6]. In Refs. [7–9], wind power generation can be improved by reasonably arranging wind turbines to minimize wake effect. The multi-body dynamic model of offshore wind turbine when considering wake effect was established in [10], in which the improved Jensen model was used to describe the wake profile. Ref. [11] incorporated Park and Law's modifications of the popular Jensen wake model into Frandsen's simplified "wake turbulence" model, and finally achieved the goal of maximizing output power. In Ref. [12], a Particle Swarm

Optimization-Model Predictive Control (PSO-MPC) strategy was proposed, and the dynamic power model was established to reduce the unit loss. Ref. [13] presented an optimal placement of WTs in a given farm area to maximize the output power with a minimum number of turbines. Ref. [14] conducted wind power distribution according to the optimal power of each wind turbine, and improved the power of the whole wind farm. In summary, these studies mainly focused on the power generation increment of a WF by considering wake effect, and the fatigue equilibrium of wind turbine is not sufficiently considered; at the same time, there is no clear quantitative relationship for operation status between different WTs, i.e., the influence of wake effect on wind farm output power and turbulence intensity have not been considered simultaneously.

To further take the turbulence intensity into account, the fatigue analysis of WTs has been studied at home and abroad. Ref. [15] applied a comprehensive fatigue coefficient in the fatigue balance optimization of offshore wind farms. A comprehensive optimization method for the fatigue load of wind turbine components and a novel multi-objective adaptive Yin–Yang pair optimization algorithm were proposed in refs. [16,17], respectively, both of which aimed to coordinate and optimize the fatigue load distribution and active power scheduling. A time-domain simulation method of fatigue load for the offshore wind power plant based on wind wave combined load was introduced in [3]. Two simplified look-up table wind turbine active power dispatching models were proposed for relieving the computing pressure of fatigue load [18], and effectively reducing the fatigue load, separately. Based on these findings, a multi-objective optimal wind farm active power distribution strategy was presented [19]. An optimal power distribution method was adopted to balance the fatigue difference of wind turbines [20], so as to maximize output power [21] and minimize fatigue load [22]. Ref. [23] used the improved-accuracy wind farm flow models to increase the power gain and reduce the fatigue load, improving the capture of wind energy and cutting down the maintenance cost at the same time.

In the above study, the consideration of wind turbine fatigue balance was only a simple linear superposition, in which it was difficult to achieve a proper balance between fatigue balance and the maximum power output target. Therefore, this paper constructs a new bi-objective optimal wind farm energy capture (OWFEC) to pursue the maximum power output and the minimum fatigue load distribution concurrently. To address this Pareto optimization problem, the decomposition-based multi-classifier-assisted evolution algorithm (MCEA) is introduced to give high-quality optimal Pareto solutions. This algorithm uses support vector machine as the auxiliary model to solve the high-dimensional classification problem with few training samples [24]. In summary, the main motivations and innovation points of this work are given as follows:

1. The bi-level OWFEC is proposed to pursue the maximum power output and the balance of fatigue load distribution during the energy capture based on the Pareto-based optimization;
2. To rapidly acquire the high-quality Pareto optimal solutions, the decomposition-based multi-classifier-assisted evolutionary algorithm is firstly designed for the presented bi-objective OWFEC;
3. The simulations are carried out with three different scales of wind farms and compared with several familiar Pareto-based meta-heuristic algorithms to evaluate the effectiveness and performance of the proposed model and algorithm.

The rest of this work is organized as follows: Section 2 presents a wake effect superposition model based on the Jensen model [25] and a mathematical model of OWFEC; Section 3 introduces the detailed design of MCEA for OWFEC; Section 4 gives the simulation results; finally, Section 5 provides the conclusions.

2. Mathematical Model of Bi-Objective Optimal Wind Farm Energy Capture

2.1. Wake Effect

In order to quantify the wake effect between different WTs, a classical Jensen model is used to evaluate the wind speed of each WT, due to its fast calculation speed and

high accuracy for engineering requirements. As shown in Figure 1, the downwind wake wind speed, $v_{j,i}$, which is x distance downstream from wind turbine unit j in the upwind direction [26], can be calculated:

$$v_{j,i} = v_j \left[1 - \left(1 - \sqrt{1 - C_T} \right) \left(\frac{R}{R + kx} \right)^2 \right] \tag{1}$$

where $v_{j,i}$ is the wake wind speed, which is x multiplied by the diameter of wind turbine distance away from the upwind unit j; R is the wind wheel radius; v_j is the incoming wind speed; k is the wake attenuation factor; and C_T represents the thrust coefficient [27], which can be written as follows:

$$C_T = 4a(1 - a) \tag{2}$$

$$a = \frac{1 \pm \sqrt{1 - C_T}}{2} \tag{3}$$

$$C_p = 4a(1 - a)^2 \tag{4}$$

where a denotes the axial induction factor, which is generally less than 0.5 in the actual operation process of the wind motor, so the above '+' does not exist; and C_p denotes the wind energy utilization coefficient, which increases with the increase of the axial induction factor.

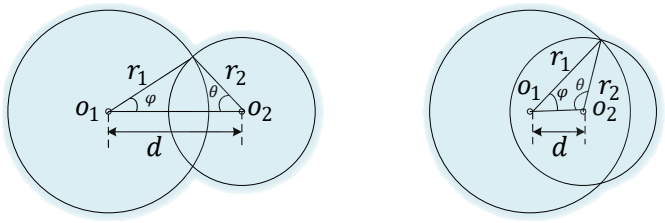

Figure 1. Intersection area between wake and wind rotor.

There are three relationships between wake radius and downwind wind wheel diameter [28]. For the case of non-intersection, it is naturally unnecessary to calculate the area of wake superposition area; for the case of complete inclusion, the wake wind speed can be calculated according to Formulas (2) or (13); for the case of partial intersection, the intersection area of wake and wind turbine needs to be calculated first, which is divided into the two cases in Figure 1.

In Figure 1, circle o_1 represents the wake area of upstream wind turbine; circle o_2 represents the wind wheel area of the downstream fan; the overlapping part represents the intersection area of the upstream wind turbine wake area and the downstream wind turbine disk. The intersection area is calculated as follows [29]:

$$A_{j,i} = arccos\left(\frac{r_1^2 + d^2 - r_2^2}{2r_1 d} \right) r_1^2 + arccos\left(\frac{r_2^2 + d^2 - r_1^2}{2r_2 d} \right) r_2^2 - sin\left(arccos\left(\frac{r_1^2 + d^2 - r_2^2}{2r_1 d} \right) r_1 d \right) \tag{5}$$

where $A_{j,i}$ represents the intersection area of the upwind unit wake area and the wind turbine area of downwind unit.

When there are $i-1$ typhoon generators set in front of wind turbine unit i, the incoming wind speed at infinity is set as v_0, and the calculation formula of wind speed v_i at wind turbine i is as follows:

$$v_i = \sqrt{v_0^2 + \sum_{j-1}^{i-1} \beta_{j,i}\left(v_{j,i}^2 - v_j^2\right)} = \sqrt{v_0^2 + \sum_{j-1}^{i-1} \beta_{j,i}\left\{v_j^2\left[1 - \frac{1-\sqrt{1-C_{T,j}}}{(1+2ks)^2}\right]^2 - v_j^2\right\}} \quad (6)$$

$$\beta_{j,i} = \frac{A_{j,i}}{\pi R^2} \quad (7)$$

where $v_{j,i}$ is the downwind wake wind speed from (1); and $\beta_{j,i}$ represents the weight of the intersection of the wake area of upstream fan j and the rotor area of downstream fan i.

It can be seen from (6) that the wind speed at downstream wind turbine i is only relevant to the thrust coefficient $C_{T,j}$ of upstream wind turbine j; changing the thrust coefficient of the upstream wind turbine can change the incoming wind speed of the downstream wind turbine.

2.2. Bi-Objective Optimization Model of OWFEC

Like the general optimization, the optimization model of OWFEC consists of two objective functions and multiple operating constraints. It attempts to realize maximization or minimization of the objective function while satisfying all the operating constraints.

2.2.1. Objective Function

The objectives of OWFEC are to maximize the output power and to minimize the standard deviation of the comprehensive fatigue coefficient. The fatigue effect of wind power is caused by changes in wind load, abnormal weather conditions, poor manufacturing and design, and improper long-term operation and maintenance. A series of measures need to be taken to reduce the risk of fatigue damage and ensure the safe operation of wind turbines. From ref. [17], we can know that the additional wake turbulence will accelerate the recovery of the wake wind speed and lead to the increase of the annual production capacity of the wind turbine; on the other hand, the additional turbulence in the wake area will increase the annual damage of the wind turbine, reduce the fatigue life of the wind turbine, and, thus, reduce the production capacity of the wind turbine over the whole life cycle. Obviously, unit active output and unit fatigue damage are a set of contradictory goals, which can be written as follows:

$$\begin{cases} max & g_1 = \sum_{i=1}^{n} \frac{1}{2}\rho\pi R^2 C_P^i(\beta,\lambda){v_i}^3 \\ min & g_2 = S[(\lambda,\beta),t] \end{cases} \quad (8)$$

where n is the number of wind turbines; ρ is the air density; R represents the radius of the wind turbine; v_i is the wind speed of the ith fan at the center of the hub; and $C_P^i(\beta,\lambda)$ represents the wind energy utilization coefficient, which is determined by the pitch angle β and tip speed ratio λ, which can be determined as follows:

$$\begin{cases} C_P^i(\beta,\lambda) = 0.5176\left[\frac{116}{\lambda_1} - 0.4\beta - 5\right] * e^{-\frac{21}{\lambda_1}} + 0.0068\lambda \\ \frac{1}{\lambda_1} = \frac{1}{(\lambda+0.08\beta)} - \frac{0.035}{\beta^3} \end{cases} \quad (9)$$

In Formula (9), $S[(\lambda,\beta),t]$ represents the standard deviation of fatigue coefficient of each unit at time t. The standard deviation of the comprehensive fatigue coefficient is used as the optimized objective in place of simply reducing the fatigue of the wind turbine [15]. In this way, the fatigue of the entire wind farm can be controlled globally, which thereby

optimizes the capacity of the wind farm and improves its economic efficiency. It can be shown as follows:

$$S[(\lambda,\beta),t] = min\sqrt{\frac{1}{n}\sum_{i=1}^{n}\{f_i[(\lambda,\beta),t] - f_{ave}[(\lambda,\beta),t]\}^2} \tag{10}$$

$$f_{ave}[(\lambda,\beta),t] = \frac{\sum_{i=1}^{n} f_i[(\lambda,\beta),t]}{n} \tag{11}$$

where $f_i[(\lambda,\beta),t]$ is the comprehensive fatigue coefficient. The traditional method of analyzing the fatigue of the wind turbine is very complicated, and it is difficult to use the operational optimization control of the whole field wind turbine. In this research, the comprehensive fatigue coefficient [30] is used to describe the damage caused by the fatigue of each component of the style power unit to the overall unit, which considers the relationship between the fatigue of each component of the unit and the active power output, which can be shown as follows:

$$f_i[(\lambda,\beta),t] = f_i[(\lambda,\beta),t_0] + \frac{\int_{t_0}^{t} P_i(t)dt}{P_{rate}^i T_{set}^i\left(1+M_{rep}^i\right)} + D_{dis}\frac{\int_{t_0}^{t} I_{eff}^i(t)dt}{T_{set}^i\left(1+M_{rep}^i\right)} \tag{12}$$

where the first subitem $f_i[(\lambda,\beta),t_0]$ indicates the fatigue coefficient of unit i at time t_0; the second subitem indicates work fatigue during power generation, so this subitem is 0 under shutdown; the third subitem represents the unit fatigue caused by turbulence; $P_i(t)$ and P_{rate}^i are the output power and rated power of unit i, respectively; T_{set}^i represents the design life; and M_{rep}^i represents the unit maintenance compensation coefficient. The compensation factor of wind turbine maintenance refers to the ratio between the expected maintenance cost and the actual maintenance cost. It is an important parameter used to measure the deviation between expected and actual maintenance costs. Generally, the maintenance compensation coefficient is a constant value, ranging from 0 to 1 based on experience [15,31–33], without detailed calculation. Additionally, in Formula (12), D_{dis} is the turbulence fatigue equivalent coefficient of wind farm. The equivalent coefficient of turbulent fatigue is used to assess the extent of damage to wind turbines in unstable wind conditions, thus helping developers and operators better manage operation and maintenance of wind farm. This coefficient is obtained by comparing the time integral of the fluctuated degree of the wind turbine blade affected by different wind speeds, wind directions, and turbulent power density in the wind farm with the time integral of the fluctuation degree of the wind turbine blade operating in the stable wind farm at the same time [15]. Finally, $I_{eff}^i(t)$ is the effective turbulence intensity of unit i at time t.

$I_{eff}^i(t)$ consists of two parts, which are the wake turbulence intensity $I_w^i(t)$ and ambient turbulence intensity $I_a^i(t)$; the calculation formula is as follows:

$$\begin{cases} I_{eff}^i(t) = \sqrt{I_a^i(t)^2 + I_w^i(t)^2} \\ I_a^i(t) = \frac{I_{ref}(0.75\cdot v_i(t)+5.6)}{v_i(t)} \\ I_w^i(t) = \frac{1}{S_i}\sqrt{1.2\cdot C_T^i(t)} \end{cases} \tag{13}$$

where I_{ref} represents the reference value of turbulence intensity when the wind speed at the hub height is 15 m/s, since the offshore wind farm is a low turbulence flow field, 0.12 is taken here; v_i is the wind speed of unit i at the hub height, m/s; S_i is the area swept by the wind turbine of unit i, m^2; and C_T^i represents the thrust coefficient of unit i.

2.2.2. Constraints

The same as the conventional wind farm scheduling problem, the obtained solution of OWFEC should satisfy various constraints, including wind speed constraint, power constraint [34], the rotor speed constraint [35], the tip speed ratio (TSR) constraint [36], and the axial induction factor constraint [37], which can be described as follows:

- Wind speed constraint: v_i is the exotic wind speed, which should be between the cut-in wind speed and the cut-off wind speed of the wind turbine, to keep the rotor of the wind turbine in operation. In this paper, wind speed scale is set as follows:

$$v_{in}^{i} \leq v_i \leq v_{out}^{i} \tag{14}$$

where v_{in}^{i} and v_{out}^{i} is respectively the cut-in and cut-off wind speed of the ith fan;

- Power constraint: P_i is the active output of the ith fan. In the traditional sense, the power can be reduced to zero through pitch regulation, and the maximum power is usually the rated power. This can be shown as follows:

$$0 \leq P_i \leq P_{rate}^{i} \tag{15}$$

where P_{rate}^{i} is the rated power of the ith fan;

- Rotor speed constraint: ω_i is the rotor speed of the ith wind turbine. The output power of a wind turbine does not exhibit linear growth with the increasing rotor speed of wind turbine. Generally, we need to keep the rotor speed within a certain range to maximize the output power. In this paper, the scale of rotor speed is set as follows:

$$\omega_0^{i} \leq \omega_i \leq 1.2 \cdot \omega_{rate}^{i} \tag{16}$$

where ω_0^{i} is the initial rotor speed of the ith fan; and ω_{rate}^{i} is the rated rotor speed of the ith fan. In this paper, we take 1.2 times the rated rotor speed as the maximum allowable rotor speed;

- Tip speed ratio (TSR) constraint: We know that $\lambda = \frac{\omega_r R}{v}$; when the pitch angle is constant, we require the wind energy utilization coefficient curve to run on the right half, so there is a minimum limit on the tip speed ratio:

$$\lambda_i \geq \lambda_{min}^{i} \tag{17}$$

where λ_i represents the tip speed ratio of the ith fan; and λ_{min}^{i} is the minimum tip speed ratio of the ith fan. Figure 2 shows the relationship between the wind energy utilization coefficient and the tip speed ratio;

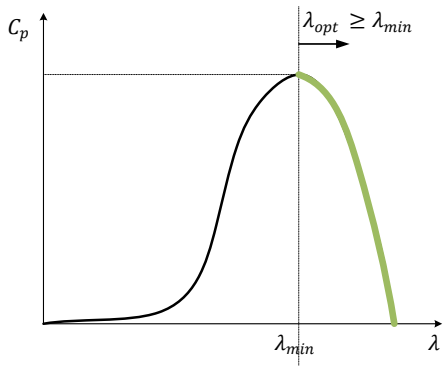

Figure 2. Relationship between C_p and λ under rated wind speed.

- Axial induction factor constraint: The axial induction factor a of wind turbines should be between 0 and $\frac{1}{3}$ because the maximum value of C_p will be obtained while a is in this range according to (4), which can be written as follows:

$$0 \leq a \leq \frac{1}{3} \tag{18}$$

3. Objective Optimization of Decomposition-Based Multi-Classifier-Assisted Evolutionary Algorithm

The core idea of MCEAD is to decompose the multi-objective problem into a group of single-objective sub-problems or multi-objective sub-problems, and optimize all sub-problems in a cooperative way by using the neighborhood relationship between sub-problems, so as to find the approximation of the whole Pareto surface. Usually, the definition of sub-problems is determined by weight vectors, and the neighborhood relationship between sub-problems is determined by calculating Euclidean distance between weight vectors. MCEAD algorithm emphasizes selecting the parent from the domain to generate new individuals through crossover operation, and carries out population updating in the domain according to certain rules. Therefore, neighborhood-based optimization strategy is an important feature to ensure the search efficiency of MCEAD. In the process of evolution, once a high-quality solution to a sub-problem is found, its good genetic information will quickly spread to other individuals in the neighboring region, thus accelerating the convergence rate of the population.

3.1. Design of the Fitness Functions

Firstly, the optimization variables are tip speed ratio λ and pitch angles β of all wind turbines, which can be expressed as $\lambda_i = \{\lambda_1, \cdots, \lambda_n | n \in N^*\}$, $\beta_i = \{\beta_1, \cdots, \beta_n | n \in N^*\}$, where n indicates the number of fan units. Initialization of optimization variables is as follows:

$$\begin{cases} \lambda_i = \frac{\omega_i r_i}{v_i} \\ \beta_i = 0 \end{cases} \tag{19}$$

where ω_i is the rotational angular velocity of the ith fan; r_i is the radius of wind wheel of the ith fan; and v_i is the incoming wind speed of the ith fan. The lower and upper bounds of all the optimization variables are set according the actual situation of the fans.

Secondly, we wanted the output power of the wind turbine to be as large as possible, and the standard deviation of turbulence intensity of the wind turbine to be as small as possible, so the two are in an opposite relationship. Therefore, we designed the following fitness function and solved it with an optimization algorithm in the subsequent content:

$$\begin{cases} f_1 = P_r - g_1 + C_f \\ f_2 = g_2 + C_f \end{cases} \tag{20}$$

where P_r is the approximate total output power of all fans; and C_f is a penalty factor, which is used when the rotor speed constraint and tip speed ratio constraint are not satisfied

3.2. Algorithm Solution

To begin with, its basic data structure and mathematical notions are as shown in Table 1.

Table 1. The basic data structure and mathematical notions.

Symbol or Expression Descriptions	Mathematical Notions
weight vector set (define Chebyshev problem)	$\{\lambda^1, \cdots, \lambda^N\}$
reference point	$z = \{z_1, \cdots, z_M\}$
a current evolutionary population	P
the weight vector set	$\{x^1, \cdots, x^N\}$
a set including N solutions	$\mathcal{P} = \left\{x^i\right\}_{i=1}^{N}$
an archive set consisting of all evaluated solutions and their objective values	$\mathcal{A}$
evaluated solutions	$x \epsilon \mathbb{R}^D$
objective values	$\{f_1(x), \cdots, f_M(x)\}$
the sub-problem area	$NS_1, \cdots, NS_N$
training samples	$\left(x_j^i, c_j^i\right)$
a dataset consisting of training samples designed for ith sub-problem	$\mathcal{D}_i$
a set of current best solutions of sub-problems for the ith sub-problem	$\mathcal{C}_i$
a set of candidate solutions of offspring $\mathcal{Y}^i$ for ith sub-problem	$\mathcal{Y}_i$
a decision function for ith sub-problem	$c_i^*(x)$
Lagrange multipliers	$\left\{a_j^{i*}\right\}_{j=1}^{\lvert\mathcal{D}_i\rvert}$
a decision score function determined with Lagrange multipliers	$d_i^*(x)$
the maximum repeat time to control the number of candidate solutions	R_{max}
the elite population used to preserve Pareto solutions	EP

Other symbols not described will be defined after the specific formula.

3.2.1. Initialization

1. The set of an elite solution set EP for holding Pareto solutions is set to an empty set $\emptyset$;

2. For each weight, determine its T closet weight vectors $\lambda^i \forall i \in \{1, \cdots, N\}$;

3. Then, initialize the population $x^1, \cdots, x^N$, and calculate each target vector value, expressed as follows:

$$\begin{array}{ll} min & F(x) = \{f_1(x), \cdots, f_M(x)\} \\ s.t. & x \in S \end{array} \tag{21}$$

where $x \in S$ denotes a decision vector x which belongs to a feasible region S, and $F(x)$ is a set of M objective functions, f_j, with $M \geq 2$. This manuscript considers real-value optimization problems with $x \in R^D$, where D is the number of decision variables. In this manuscript, we use the Chebyshev function as a scalarization function to divide a particular problem into N sub-problems, where the ith scalarization function is expressed as follows:

$$g\left(x\middle|\lambda^i, z\right) = \max_{1 \leq j \leq M}\left\{\lambda_j^i \middle| f_j(x) - z_j\right\} \tag{22}$$

where $\lambda^i = \{\lambda_1^i, \cdots, \lambda_M^i\}$ is a weight vector; and $z = \{z_1, \cdots, z_M\}$ is a set of reference points determined as the optimal value of each objective function;

4. Lastly, initialize the current reference point, $z_j = min_{i \in \{1, \cdots, N\}} f_j\left(x^i\right) \forall j \in \{1, \cdots, M\}$.

3.2.2. Update Operations

For each $i \in \{1, \cdots, N\}$, perform the following steps:

1. Each sub-problem has individual crossover and mutation in the neighborhood. MCEAD defines an index set of neighbor sub-problems for the ith one, denoted by $B(i)$, and the index set of parent candidates, P, can be expressed as follows:

$$P = \begin{cases} B(i) & with\ a\ probility\ \delta \\ \{1, \cdots, N\} & otherwise \end{cases} \tag{23}$$

Additionally, the process of crossover and mutation are as follows:

$$\mathcal{Y}_k^i = \begin{cases} x_k^i + F \times \left(x_k^{r_1} - x_k^{r_2}\right) & with\ probility\ CR \\ x_k^i & otherwise \end{cases} \tag{24}$$

$$\mathcal{Y}_k^i \leftarrow \begin{cases} \mathcal{Y}_k^i + \sigma_k \times (b_k - a_k) & with\ probility\ p_m \\ \mathcal{Y}_k^i & otherwise \end{cases} \tag{25}$$

where $\mathcal{Y}_k^i$ is a kth decision variable of $\mathcal{Y}^i$; F and CR are scaling factor and crossover rate, respectively; p_m is a mutation probability; and a_k and b_k are the lower/upper bounds of the kth decision viriable. σ_k is further expressed as follows:

$$\sigma_k = \begin{cases} (2r)^{1/(\eta+1)} - 1 & if\ r\ <\ 0.5 \\ 1 - (2 - 2r)^{1/(\eta+1)} & otherwise \end{cases} \tag{26}$$

where η is a distribution index of polynomial mutation and $r >\in [0, 1]$ is a uniformly-sampled random value;

2. For each sub-problem, build a decision function $c_i^*(x)$ which generates an offspring solution $\mathcal{Y}^i$, each of which is denoted by model-construction and solution-generation. Subsequently, $\mathcal{Y}^i$ is inserted to $\mathcal{A}$;

3. After completing the calculation of $\mathcal{Y}_k^i$ for all $k = 1, \cdots, D$, $\mathcal{Y}^i$ is evaluated with the fitness functions in Formula (20);

4. Update reference points $z = \{z_1, \cdots, z_m\}$;

5. For each $j \in NS_i$, if $g\left(\mathcal{Y}^i \middle| \lambda^j, z\right) \leq g\left(x^j \middle| \lambda^j, z\right)$, perform the replacement $x^j = \mathcal{Y}^i$, and update the individual in the domain, where x^j is the individual in the jth weight sub-problem;

6. Update the archive set $\mathcal{A}$;

7. Update the external set EP.

3.2.3. Termination of the Judgement

If the termination condition is met, the outer set EP is output; otherwise, turn to process *ii*.

3.3. Calculation Flow

The whole calculation flow of solving the multi-objective optimization model of wind farm is provided in Algorithm 1, where the termination condition of MCEAD is set to the maximum iteration number. For each sub-problem, MCEAD builds a decision function $c_i^*(x)$, and then it generates an offspring solution $\mathcal{Y}^i$ by using $c_i^*(x)$, which are denoted by model-construction at line 11 and solution-generation at line 13. The following steps describe the detailed procedure of model-construction and solution-generation.

Algorithm 2 describes the complete procedure of model-construction. For the ith sub-problem, MCEAD builds a dataset $\mathcal{D}_i$, which is designed such that $c_i^*(x)$ captures a good region, which may improve $g\left(x \middle| \lambda^i, z\right)$, together with its neighbor scalarization functions. In addition, each $c_i^*(x)$ may be similar to, but still different from, ones built for neighboring sub-problems. Accordingly, each sub-problem is conservatively explored via different surrogate models. For the establishment of SVM classifier model, we have made a special treatment, and we add the sub-best solution to $\mathcal{C}_i$ to avoid duplicative selection. With this exception handling, it is guaranteed that $\mathcal{D}_i$ always includes a fixed number of

positive samples. Accordingly, the number of negative samples will increase, which is more helpful to build a special agent model for sub-problems.

Algorithm 1: MCEAD for OWFEC

Input: $N, T, \{\lambda^1, \cdots, \lambda^N\}, F, CR, \eta, p_m, n_r, \delta, \gamma, C, R_{max}$;
Output: EP;
Initialize EP as $EP \leftarrow \varnothing$; (19);
Set $\boldsymbol{B}(i)$ to indices of the T closest weight vectors to $\lambda^i \forall i \in \{1, \cdots, N\}$;
Set $\mathcal{P}$ to initial solutions $\{x^1, \cdots, x^N\}$;
Evaluate $\forall x \in \mathcal{P}$;
Initialize z_j as $z_j \leftarrow min_{x \in \mathcal{P}} f_j(x) \forall j \in \{1, \cdots, M\}$;
Initialize $\mathcal{A}$ as $\mathcal{A} \leftarrow \mathcal{P}$;
While termination criteria are not met **do**
    for $i = 1$ to N **do**
        Build surrogate as $c_i^*(x) \leftarrow$ model-construction $\left(\mathcal{A}, \lambda^i\right)$;
        Set $\boldsymbol{P}$; (23);
        Generate $\mathcal{Y}^i$ as $\mathcal{Y}^i \leftarrow$ solution-generation $\left(\mathcal{P}, \boldsymbol{P}, c_i^*(x)\right)$; (24–25);
        Evaluate $\mathcal{Y}^i$; (8–13, 20)
        Update $z_j \leftarrow \min\left\{z_j, f_j\left(\mathcal{Y}^i\right)\right\} \forall j \in \{1, \cdots, M\}$; (22)
        Randomly shuffle indices of $\boldsymbol{P}$;
        count$\leftarrow$0;
        for each $j \in \boldsymbol{P}$ **do**
            if $g\left(\mathcal{Y}^i \middle| \lambda^j, z\right) \leq g\left(x^j \middle| \lambda^j, z\right)$ and count $< n_r$ **then**
                $x^j \leftarrow \mathcal{Y}^i$;
                count $\leftarrow$ count+1;
            end if
        end for
        Update $\mathcal{A}$ as $\mathcal{A} \cup \left\{\mathcal{Y}^i\right\}$;
        Remove from EP all the solutions dominated by $\mathcal{Y}^i$;
        Add $\mathcal{Y}^i$ to EP if $\mathcal{Y}^i$ is the Pareto solution in EP;
    End for
End while

Algorithm 2: Model-Construction

$D_i, C_i \leftarrow \varnothing, \varnothing$;
for each $k \in B(i)$ **do**
    $x_k^* \leftarrow arg \quad min_{x \in \mathcal{A} \wedge x \notin \mathcal{C}_i} g\left(x \middle| \lambda^k, z\right)$;
    $\mathcal{C}_i \leftarrow \mathcal{C}_i \cup \{x_k^*\}$;
end for
for each $x \in \mathcal{A}$ **do**
    if $x \in \mathcal{C}_i$ **then**
        $\mathcal{D}_i \leftarrow \mathcal{D}_i \cup \{(x, +1)\}$;
    else
        $\mathcal{D}_i \leftarrow \mathcal{D}_i \cup \{(x, -1)\}$;
    end if
end for
$c_i^*(x) \leftarrow$ *build the decision function trained with* $\mathcal{D}_i$;
return $c_i^*(x)$

In Algorithm 3, we use the model to predict whether the candidate solution has the positive class. If there is still no positive predictive solution after the maximum repeat time R_{max} is reached, we will select some points closest to a decision boundary drawn by $c_i^*(x)$ among the existing solutions to make our solution close to the optimal solution plane.

Algorithm 3: Solution-Generation

$\mathcal{Y}_i \leftarrow \emptyset$;
for r = 0 to R_{max} **do**
  $\hat{\mathcal{Y}}^i \leftarrow$ *generate a candidate*;
  if $c_i^*\left(\hat{\mathcal{Y}}^i\right) = +1$ **then**
    $\mathcal{Y}^i \leftarrow \hat{\mathcal{Y}}^i$;
    return $\mathcal{Y}^i$;
  else
    $\mathcal{Y}_i \leftarrow \mathcal{Y}_i \cup \left\{\hat{\mathcal{Y}}^i\right\}$;
  end if
end for
$\mathcal{Y}^i \leftarrow arg \quad max_{\hat{\mathcal{Y}}^i \in \mathcal{Y}_i} d_i^*\left(\hat{\mathcal{Y}}^i\right)$;
return $\mathcal{Y}^i$

3.4. Overall Execution Procedure

To this end, the overall execution procedure of wind power dispatching optimization-based MCEAD is depicted in Figure 3.

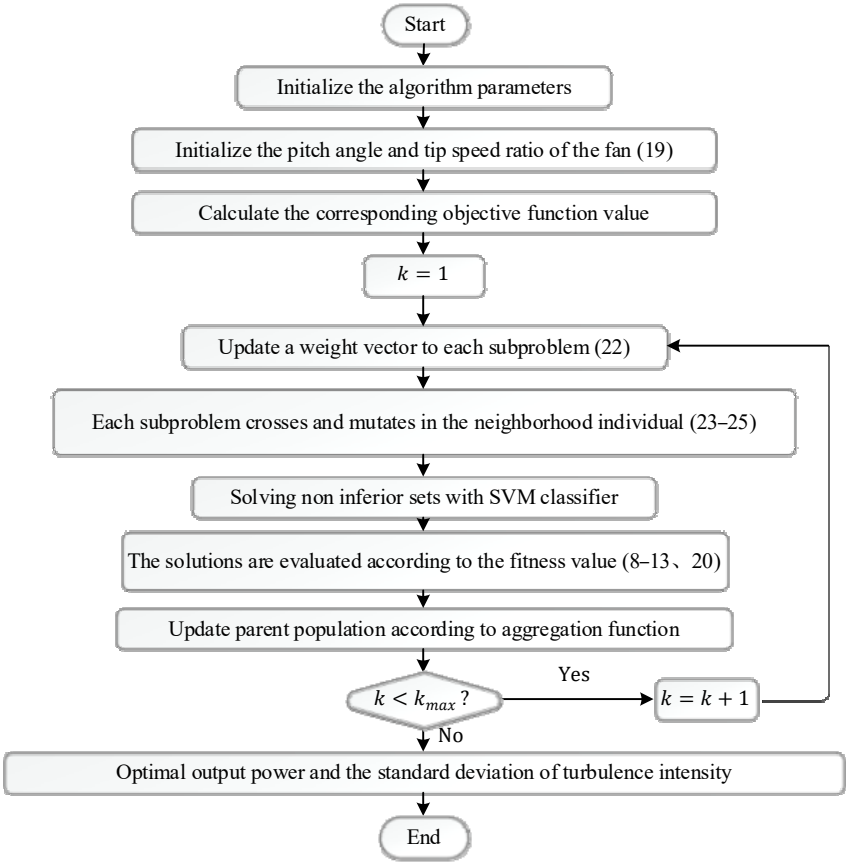

Figure 3. Overall execution procedure of wind power dispatching optimization-based MCEAD.

3.5. Best-Compromise Solution

In practice, the final implementation of the scheme is usually only one; therefore, the decisionmaker needs to choose an optimal compromise solution from the Pareto optimal solution set. Here, the optimum compromise solution can be determined according to the fuzzy set theory. The satisfaction degree corresponding to each objective function in

each Pareto solution can be expressed by the fuzzy membership function, which is defined as follows:

$$h_i = \begin{cases} 1 & f_i \le f_i^{min} \\ \frac{f_i^{max} - f_i}{f_i^{max} - f_i^{min}} & f_i^{max} > f_i > f_i^{min} \\ 0 & f_i \ge f_i^{max} \end{cases} \quad (27)$$

where $i \in \left\{1, 2, \cdots, N_{obj}\right\}$; f_i is the objective function; N_{obj} is the number of the objective function; and f_i^{max} and f_i^{min} are the maximum and minimum values of the ith objective function, respectively. When h_i is 0 or 1, the ith objective function value is completely dissatisfied or completely satisfied, respectively. The standardization satisfaction degree of each solution in the Pareto solution set can be obtained as follows:

$$h = \frac{1}{N_{obj}} \quad (28)$$

4. Case Studies

The proposed wind power dispatching optimization model with MCEAD algorithm is evaluated in this section. Three simulations are used to illustrate the optimization effects of different algorithms, including NSGA, MOPSO, SPEA2, MOGWO, MOEADDE, and NSGAIII. Specifically, the Pareto solution set of OWFEC can be obtained by using different algorithms under different incoming wind directions (including spatial evaluation method, super volume index, solution set coverage, etc.). Then, the compromise solution, average value, and minimum value of each solution set are visually displayed as the optimization results of each algorithm. Meanwhile, the average value of each solution set is placed in the Pareto solution set determined by MCEAD for comparison. In case 1, we consider 10 WTs under 90° and 270° inflow wind directions. Similarly, 50 WTs with the incoming wind directions 10° and 100° are tested in case 2. In case 3, the number of fans has changed to 100, and the dimension of decision-making space has been increased many times compared to the first two cases. In addition to similar results in the previous cases, the operation time has also been compared in case 3. Some parameters in the simulations are set as shown in Table 2.

Table 2. The main parameters of OWFEC for each Case.

Parameters	Value
Number of fans	10 (Case 1) 50 (Case 2) 100 (Case 3)
Wind wheel radius (m)	33 (Case 1) 30.5 (Case 2 and 3)
Wind wheel speed (rad/s)	3.5
Rated wind speed (m/s)	12
Decay coefficient	0.04
Spacing between fans (m)	300
P_r (kW)	15 (Case 1) 75 (Case 2) 150 (Case 3)
Population number	100 (Case 1) 200 (Case 2 and 3)
Number of iterations	50

The specific test results are shown as follows:

1. In case 1, 10 fans are uniformly arranged with the given wind speed and fan rotation angular velocity. The OWFEC is explored by changing the inflow wind speed, as the inflow angle has a great influence on the output power and fatigue damage of the fan, with the simulation results being shown in Figure 4. This shows the MCEAD has the most beautiful

Pareto preface in solving the model, in which its convergence speed and solution diversity are better. In addition, it can find a better compromise solution within the target time, and realize the collective optimization of two objectives. The specific test data are shown in Table 3.

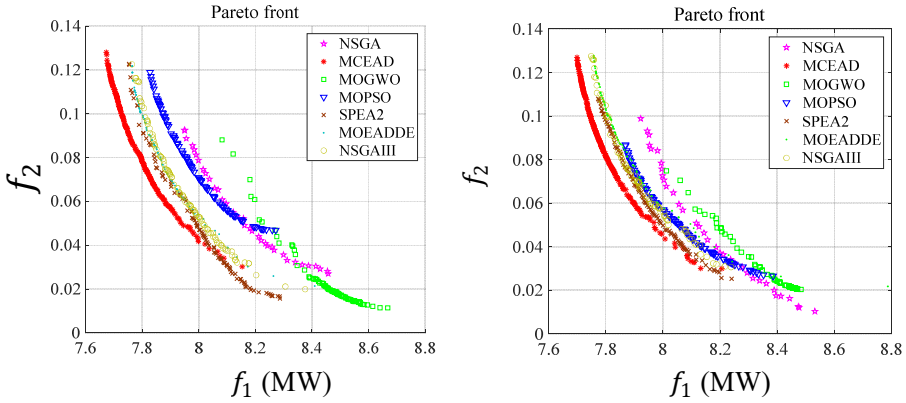

Figure 4. Comparison of Pareto fronts by different multi-objective optimization algorithms for model solving under 90° (**left**) and 270° (**right**) wind direction.

Table 3. Run results of different algorithms for 10 fans under 90° and 270° inflow wind direction.

Wind Direction (°)	Algorithm	Best-Compromise Solution		Average Value		Minimum Value		Spacing	HV
		f_1 (MW)	f_2	f_1 (MW)	f_2	f_1 (MW)	f_2		
90°	NSGA	8.4576	0.0270	8.1724	0.0542	7.9490	0.0270	0.0057	1.4971
	MCEAD	8.1534	0.0302	7.7882	0.0860	7.6732	0.0302	0.0051	2.1077
	MOGWO	8.6679	0.0114	8.4577	0.0233	8.0823	0.0114	0.0078	1.3859
	MOPSO	8.2722	0.0469	8.0008	0.0760	7.8276	0.0469	0.0025	1.5841
	SPEA2	8.2870	0.0157	8.0124	0.0506	7.7533	0.0157	0.0032	1.7009
	MOEADDE	8.4100	0.0214	7.8764	0.0823	7.7647	0.0241	0.0195	1.6794
	NSGAIII	8.3760	0.0199	7.9557	0.0657	7.7638	0.0199	0.0103	1.6827
270°	NSGA	8.5321	0.0103	8.1780	0.0484	7.9226	0.0103	0.0104	1.5417
	MCEAD	8.2065	0.0299	7.8030	0.0874	7.6999	0.0300	0.0054	1.7316
	MOGWO	8.4835	0.0204	8.3912	0.0279	8.0127	0.0204	0.0077	1.4456
	MOPSO	8.3861	0.0265	8.0660	0.0523	7.8692	0.0265	0.0044	1.5774
	SPEA2	8.2409	0.0253	7.9505	0.0640	7.7737	0.0253	0.0040	1.6688
	MOEADDE	8.7874	0.0218	7.8826	0.0890	7.7585	0.0218	0.0427	1.6784
	NSGAIII	8.2065	0.0300	7.8030	0.0874	7.6999	0.0300	0.0054	1.6816

In Table 3, the spacing value of MCEAD is almost equal to 0, which is smaller than that obtained by other algorithms. This indicates that the solution set of MCEAD is more evenly-distributed in the target space. Meanwhile, the vector [9.5 1] is selected as the reference vector, and its hypervolume is the largest, indicating that it is closer to the ideal Pareto front. The compromise solution, average value, and minimum value obtained by each algorithm are shown as Figure 5. In addition, the Pareto solution set obtained by MCEAD is taken as the benchmark solution, and the average value of solution sets of each group is compared in Figure 6.

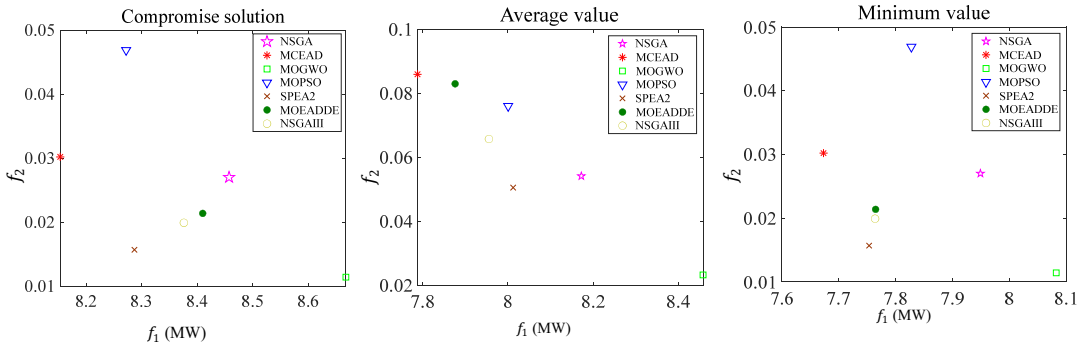

Figure 5. Comparison of three types of solutions by different multi-objective optimization algorithms for model solving (10 units under 90°).

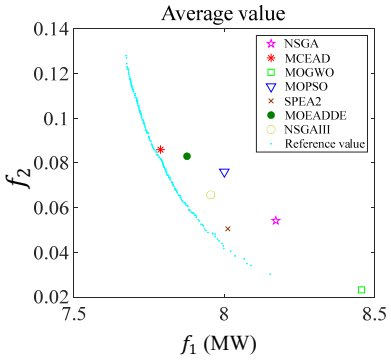

Figure 6. Comparison of average value by different multi-objective optimization algorithms for model solving (10 units under 90°).

Next, the inflow direction is changed to 270°, while other operating conditions are maintained. In this case, MCEAD also has the largest hypervolume. The compromise solution, average value, and minimum value obtained by each algorithm are shown in Figure 7. Similarly, based on the Pareto front of MCEAD, the average solution distribution of each algorithm is shown in Figure 8. It can be seen that the average value of MCEAD is the closest to the reference value, meaning it can capture a better solution for the overall power generation process of the wind turbine. In addition, the coverage of the C-metric solution set obtained by each algorithm is shown in Table 4, in which the solution set generated by MCEAD is better than those obtained by other algorithms. Overall, MCEAD remains optimal in searching for an optimal solution to the OWFEC problem, even if the inflow wind direction is changed;

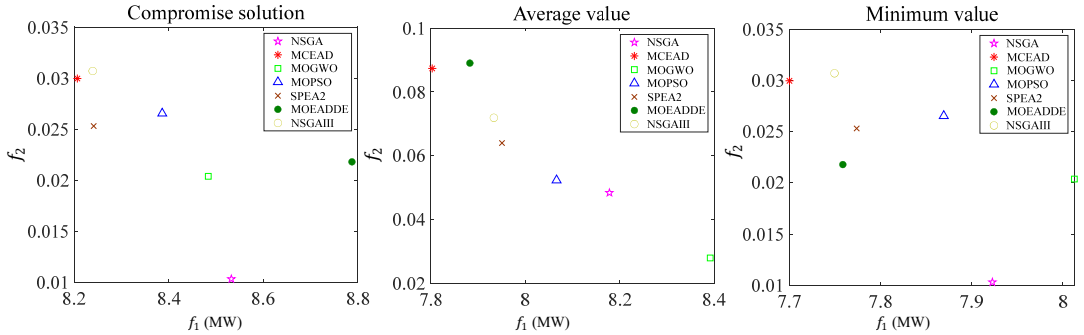

Figure 7. Comparison of three types of solutions by different multi-objective optimization algorithms for model solving (10 units under 270°).

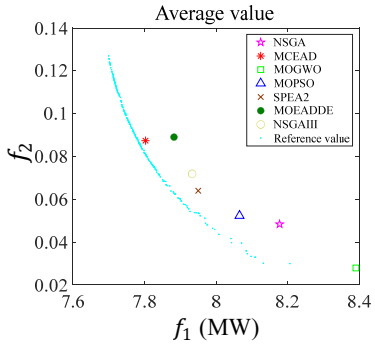

Figure 8. Comparison of average value by different multi-objective optimization algorithms for model solving (10 units under 270°).

Table 4. Comparison of C-metric solution sets obtained by each algorithm.

Wind Direction (°)	Compare Objects	NSGA	MOGWO	MOPSO	SPEA2	MOOEADDE	NSGAIII
90°	C (A, B)	0.9143	0.1500	1	0.1700	0.9462	0.7600
	C (B, A)	0	0	0	0.4587	0.0046	0.0413
270°	C (A, B)	0.6857	0.2400	0.9200	0.9000	0.9789	1
	C (B, A)	0	0	0	0.0044	0	0

Note: A represents the solution set of MCEAD algorithm, and B represents the solution set of other algorithms; when C (A, B) is greater than C (B, A), it means that Pareto solution set A is better than B for the same problem.

2. In case 2, the number of fans is increased to 50 and the inflow wind speed angle β is set as 10° or 100°, while other conditions are unchanged from case 1. When the inflow wind speed angle β is 10°, the output results of fan output power and standard deviation of comprehensive fatigue coefficient optimized by these five algorithms are as shown in Figure 9. Comparison results are in Figure 10, with the angle of inflow wind speed adjusted to 100°.

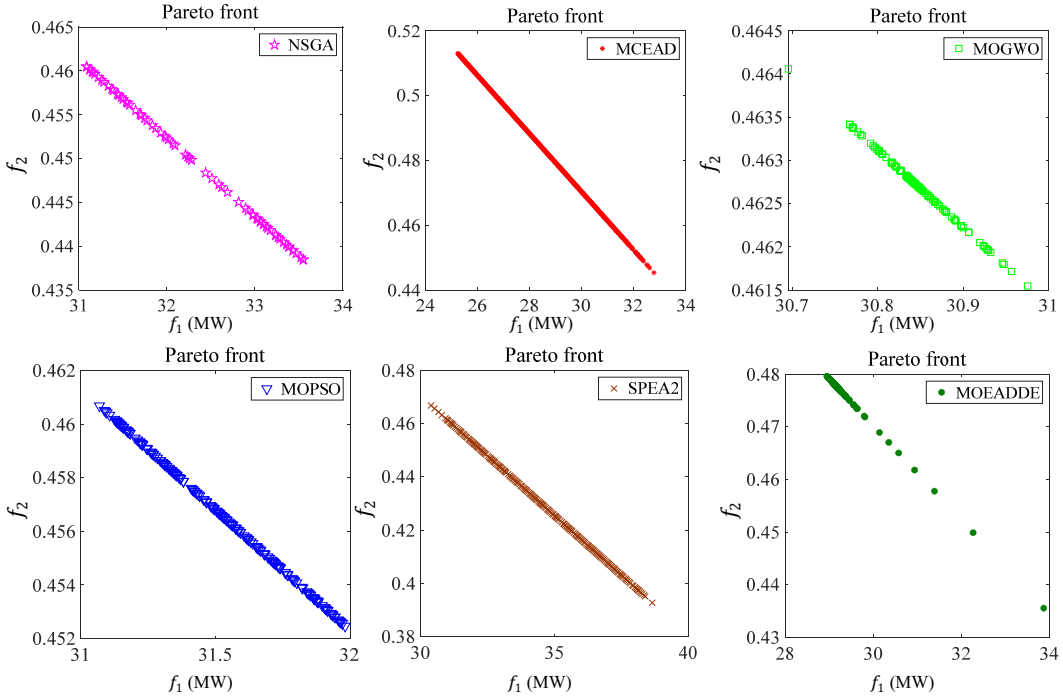

Figure 9. Comparison of Pareto front by different multi-objective optimization algorithms for model solving (10°).

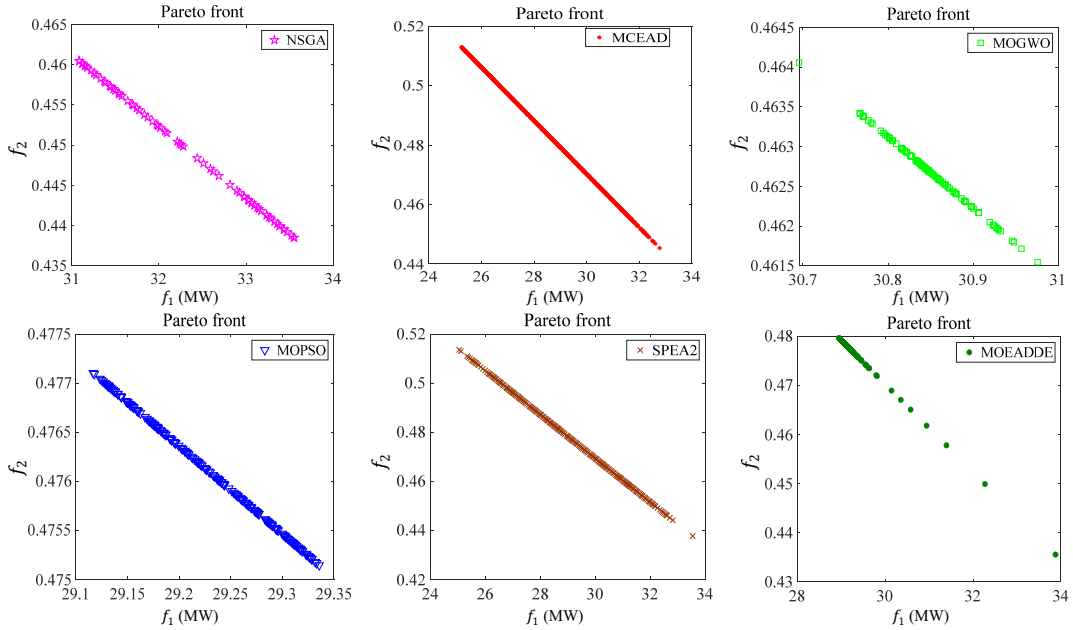

Figure 10. Comparison of Pareto front by different multi-objective optimization algorithms for model solving (100°).

It can be seen from the above two test charts that MCEAD can always capture larger output power and smaller standard deviation, even if the inflow wind direction is changed. MCEAD shows better convergence speed and stability for optimizing high-dimensional multi-objective problems. This is because adding an agent model can greatly shorten optimization time when optimizing high-dimensional optimization problems, leading to the optimization results being more prominent than other traditional multi-objective algorithms. The specific test data are shown in Table 5. The solution set of MCEAD has a much larger HV than that of other algorithms, which shows the superiority of MCEAD in solving this bi-objective optimization problem. From the results, we can also see that the change in target 2 is generally small, so we can focus on comparing the change range of target 1, as shown Figure 11. Figure 12 shows the comparison of power difference captured by different algorithms relative to MCEAD. The coverage of the C-metric solution set obtained by each algorithm under 10° inflow direction is shown in Table 6, which shows that the solution set obtained by MCEAD is more dominant than all other test algorithms;

Table 5. Run results of different algorithms for 50 fans under 10° and 100° inflow wind direction.

Wind Direction (°)	Algorithm	Best-Compromise Solution		Average Value		Minimum Value		Spacing	HV
		f_1 (MW)	f_2	f_1 (MW)	f_2	f_1 (MW)	f_2		
10°	NSGA	33.5481	0.4385	32.3184	0.4495	31.0872	0.4385	0.0178	6.1002
	MCEAD	32.7725	0.4453	27.8147	0.4899	25.2341	0.4453	0.0030	9.0438
	MOGWO	30.9756	0.4615	30.8464	0.4627	30.6954	0.4615	0.0074	6.0866
	MOPSO	31.5286	0.4565	31.5286	0.4565	31.0694	0.4525	0.0023	5.9811
	SPEA2	38.6547	0.3928	34.5427	0.4296	30.3903	0.3928	0.0219	6.7422
	MOEADDE	33.8762	0.4355	29.2674	0.4768	28.9505	0.4355	0.1449	7.2399
100°	NSGA	29.3697	0.4749	28.2142	0.4852	26.9804	0.4749	0.0118	7.8611
	MCEAD	28.1785	0.4854	23.9225	0.5235	20.9216	0.4855	0.0017	10.5824
	MOGWO	29.3631	0.4751	28.8667	0.4795	28.2334	0.4750	0.0141	7.2210
	MOPSO	29.3356	0.4752	29.2265	0.4761	29.1167	0.4751	0.0028	6.7616
	SPEA2	33.5379	0.4377	29.0723	0.4775	25.0409	0.4377	0.0507	9.2101
	MOEADDE	29.0214	0.4780	24.8235	0.5155	24.3680	0.4780	0.1769	7.2399

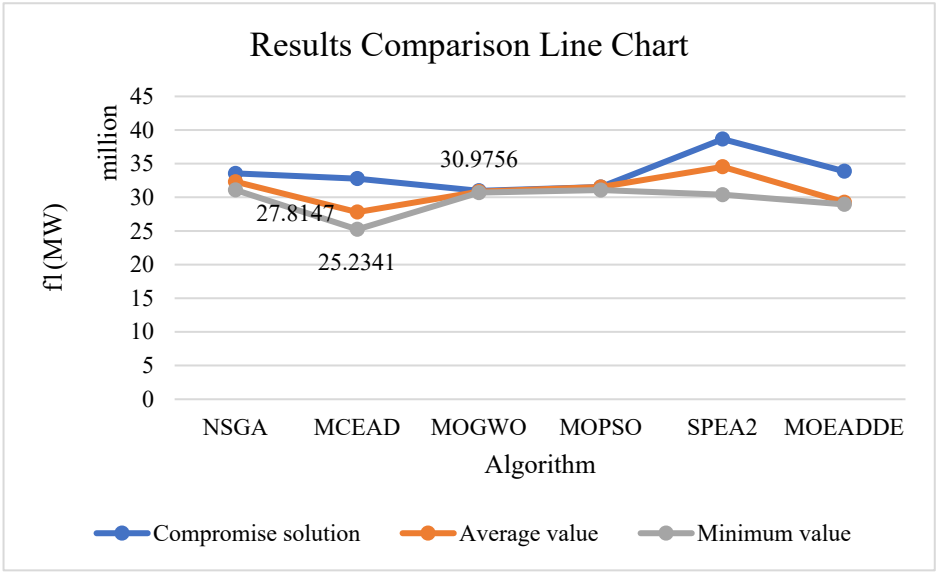

Figure 11. Comparison diagram of target 1 by 50 fans under 10° inflow direction.

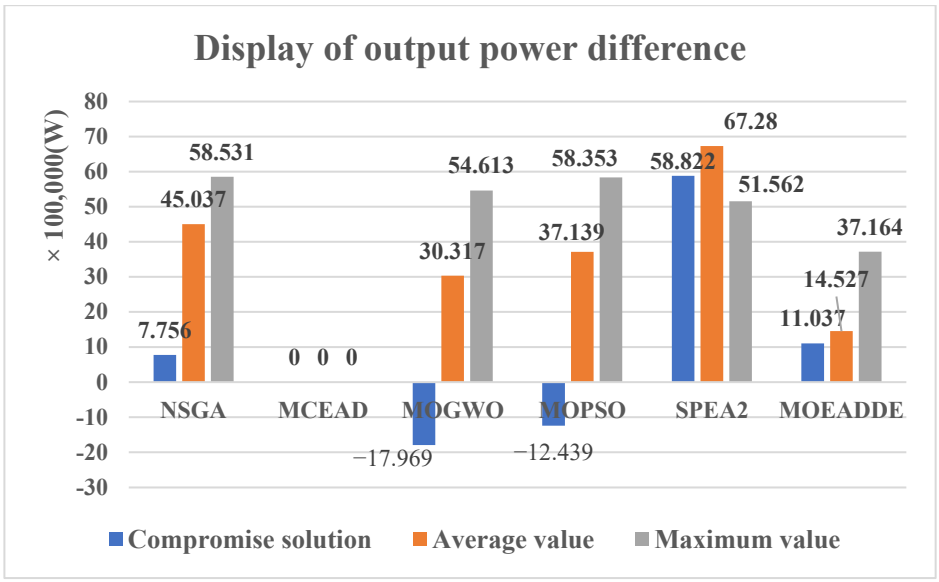

Figure 12. Difference of captured power under different algorithms by 50 fans (10°).

Table 6. Comparison of C-metric solution sets obtained by each algorithm.

Compare Objects	NSGA	MOGWO	MOPSO	SPEA2	MOOEADDE
C (A, B)	0.1286	0.7900	0.4850	0.1250	0.0166
C (B, A)	1.9932×10^{-4}	0	0	0	0

Note: A represents the solution set of MCEAD algorithm, and B represents the solution set of other algorithms; when C (A, B) is greater than C (B, A), it means that Pareto solution set A is better than B for the same problem.

3. In case 3, the number of fans is increased to 100, while the parameter settings are set as the same as those of the previous 50 fans. The comparison diagram of the final algorithm test results is shown in Figure 13. From the above results, we know that a better solution set of two targets can be found by MCEAD; the specific test data are shown in Table 7. Comparison diagram of target 1 with 100 fans under 10° inflow wind direction and different evaluating parameters for 100 fans under 10° inflow wind direction are represented in

Figures 14 and 15, respectively. The HV of the solution set obtained by MCEAD is 7.5143, which is far greater than that obtained by other algorithms. Compared with the operation of the first 10 and 50 fans, the dimension of 100 fans increases several times, and the MCEAD operation results show greater advantages, which implies the MCEAD is more proficient in dealing with higher-dimensional optimization problems. In addition, MOGWO cannot find a suitable Pareto solution set with the same population number and iteration number.

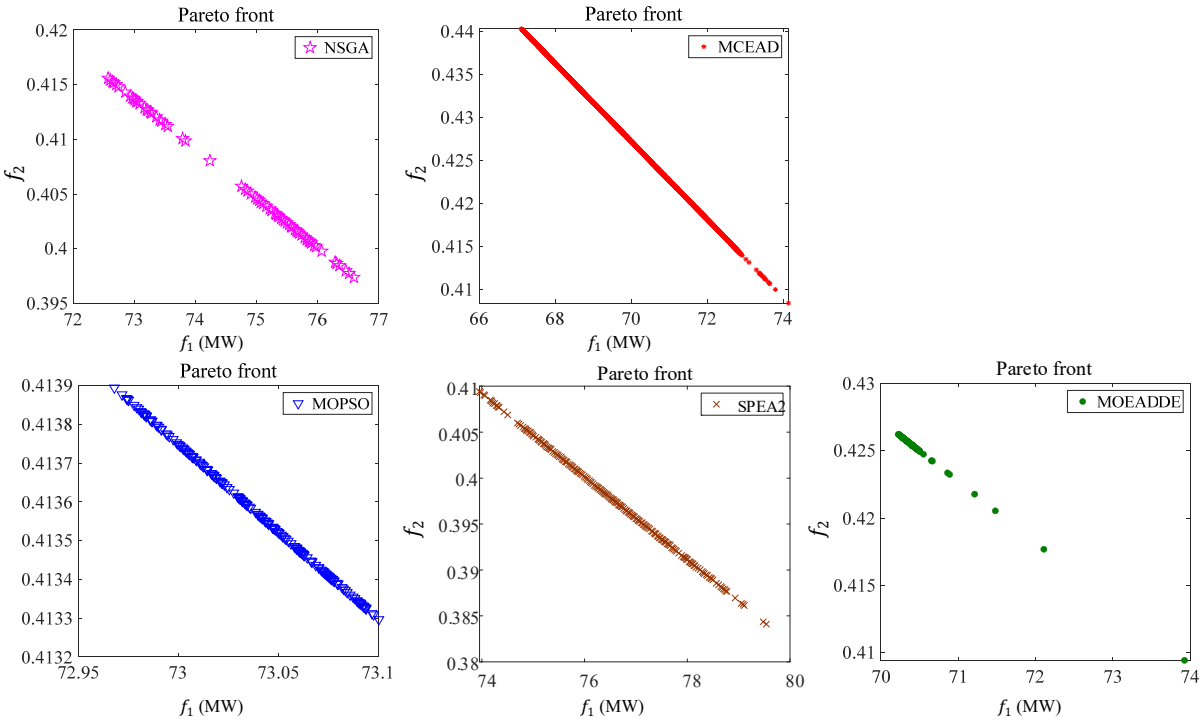

Figure 13. Comparison of Pareto front by different multi-objective optimization algorithms for model solving.

Table 7. Run results of different algorithms for 100 fans under 10° inflow wind direction.

Algorithm	Best-Compromise Solution		Average Value		Minimum Value		Spacing	HV
	f_1 (MW)	f_2	f_1 (MW)	f_2	f_1 (MW)	f_2		
NSGA	76.5911	0.3974	74.6424	0.4062	72.5716	0.3974	0.0472	4.4384
MCEAD	74.1414	0.4085	69.8633	0.4279	67.1066	0.4084	0.0070	7.5143
MOGWO	—	—	—	—	—	—	—	—
MOPSO	73.1003	0.4132	73.0380	0.4136	72.9681	0.4133	0.0034	4.1256
SPEA2	79.5391	0.3841	76.5689	0.3976	73.9552	0.3841	0.0115	3.6514
MOEADDE	73.9282	0.4095	70.4324	0.4253	70.2278	0.4094	0.1616	5.7311

MCEAD shows greater advantages for solving such high latitude problems. A good Pareto optimal solution can be found even if the population number or the number of iterations is reduced, which further reduces the time cost. After reducing the number of corresponding populations and iterations, we can get the following results in Table 8.

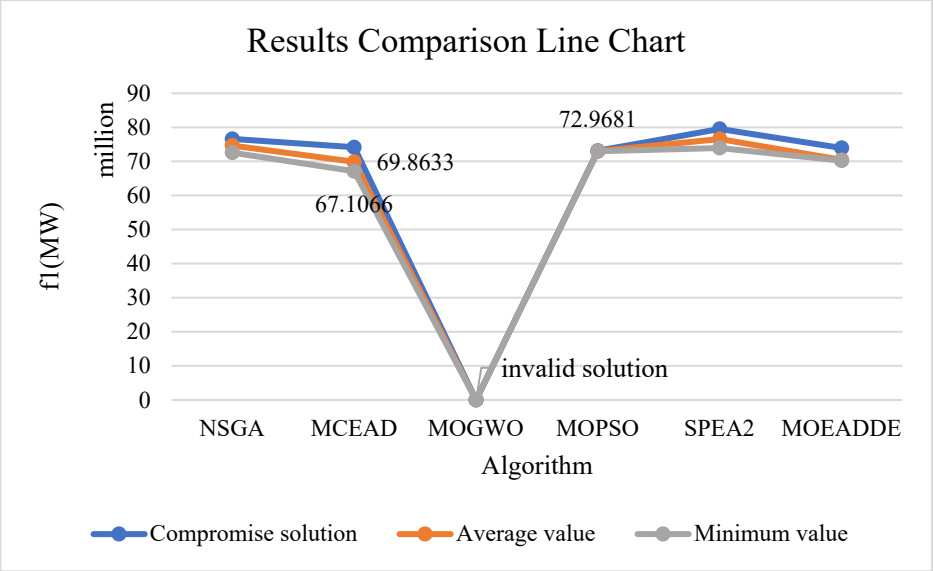

Figure 14. Comparison diagram of target 1 by 100 fans under 10° inflow wind direction.

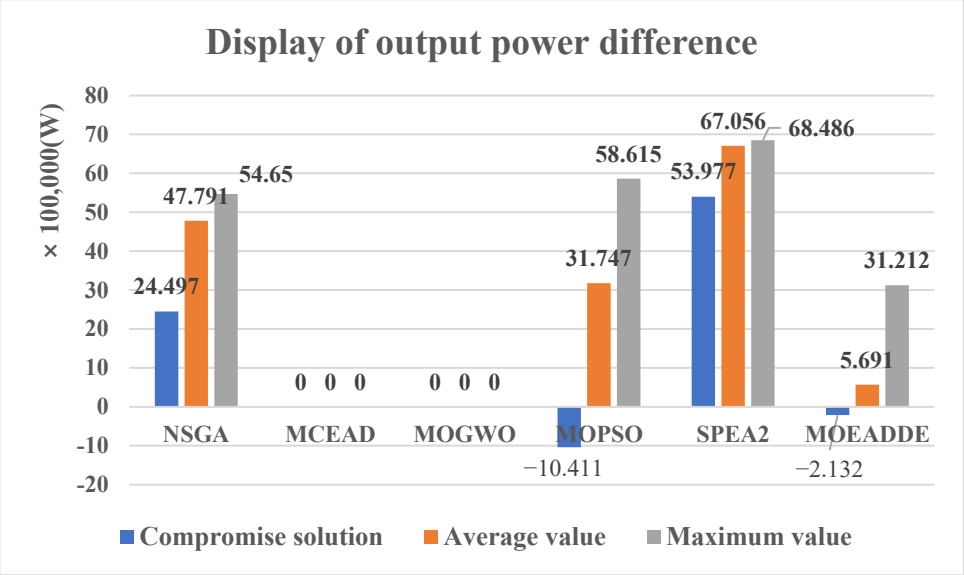

Figure 15. Capture power comparison under different algorithms (10°).

From Table 8, we can draw the conclusion that MCEAD needs more time when solving high-dimensional problems with the same population and number of iterations. We can always obtain a better solution set than with other algorithms, with faster convergence speed and bigger hypervolume, even if our function evaluations are reduced. This implies that the improved algorithm has more advantages in dealing with double-objective optimization problems such as OWFEC. The more fans, the more obvious the advantages of this algorithm.

Table 8. Comparison of different evaluating parameters for 100 fans under 10° inflow wind direction.

Algorithm	Population Number	Iterations	FEs	Average Value		Time Cost (mins)	HV
				f_1 (MW)	f_2		
NSGA	200	50	10,000	74.6424	0.4062	75.79	4.4384
MCEAD	200	50	10,000	69.8633	0.4279	192.73	7.5143
	150	50	7500	70.0236	0.3965	90.09	7.3912
	100	50	5000	71.5648	0.4029	51.43	7.1648
	50	50	2500	72.3229	0.4138	26.02	6.8562
MOGWO	400	100	10,000	74.1593	0.4087	338.89	3.6443
MOPSO	200	50	10,000	73.0380	0.4136	83.12	4.1256
SPEA2	200	50	10,000	76.5689	0.3976	85.40	3.6514
MOEADDE	200	50	10,000	70.4324	0.4253	76.20	5.7311

5. Conclusions

A novel bi-objective OWFEC model is proposed in this paper for maximizing wind power output and balancing fatigue load distribution simultaneously. The decomposition-based multi-classifier-assisted evolutionary algorithm (MCEAD) with faster and more stable convergence characteristics is used to find the optimal solution of the proposed model. Based on simulation studies, it is concluded that the proposed OWFEC model can be optimized to an appropriate solution, which reaches an equilibrium solution with more wind output power and lower standard deviation of the comprehensive fatigue coefficient. In addition, the effectiveness and advantages of high-speed and high-quality convergence of MCEAD are verified, which help the proposed model greatly improve the energy capture and economic benefits of the whole wind farm. Compared with traditional algorithms (NSGA, MOGWO, MOPSO, SPEA2, and MOEADDE) for three different scales of wind farms, both the average energy output captured and standard deviation of comprehensive fatigue coefficient of MCEAD are considerably better, and the high-dimensional optimization problem is solved better. Lastly, MCEAD reduces the maximum evaluation coefficient several times in solving the two-objective optimization problem for obtaining similar quality target solutions, which lowers various costs. The future work involves two main problems: (1) How to improve the feasibility of the algorithm in practice when larger scale wind farms are incorporated; (2) How to extend static day-ahead optimization to dynamic optimization of wind power generation prediction, to make the whole wind power system more stable and safer. In subsequent studies, the day-ahead optimization model can be extended to intraday optimization, which occurs each hour, every five minutes, or a shorter time, with dynamic optimization throughout the day [38–40]. The day-ahead optimization schedules most of the power output, while the intraday optimization acts as a compensation to deal with real time uncertainties. They are encouraged to be used in cooperation to improve the operational efficiency of wind farms.

Author Contributions: Writing—original draft, H.Z.; Writing—review & editing, X.G.; Conceptualization, L.Z.; Methodology, X.Z. All authors have read and agreed to the published version of the manuscript.

Funding: This research was funded by Shenzhen Polytechnic (the Scientific Research Startup Fund for Shenzhen High-Caliber Personnel of SZPT (No.6022310042k)), Northeastern University (Foshan Graduate School of Innovation), and Shantou University (Guangdong Basic and Applied Basic Research Foundation under Grant 2019A1515011060).

Acknowledgments: This work was jointly supported by Shenzhen Polytechnic (the Scientific Research Startup Fund for Shenzhen High-Caliber Personnel of SZPT (No.6022310042k)), Northeastern University (Foshan Graduate School of Innovation), and Shantou University (Guangdong Basic and Applied Basic Research Foundation under Grant 2019A1515011060).

Conflicts of Interest: The authors declare no conflict of interest.

References

1. Cui, D.; Xu, F.; Ge, W.; Huang, P.; Zhou, Y. A coordinated dispatching model considering generation and operation reserve in wind power-photovoltaic-pumped storage system. *Energies* **2020**, *13*, 4834. [CrossRef]
2. Charhouni, N.; Sallaou, M.; Mansouri, K. Investigation of wake interactions effect on wind farm efficiency. In Proceedings of the 2018 4th International Conference on Optimization and Applications (ICOA), Mohammedia, Morocco, 26–27 April 2018.
3. Yao, Q.; Liu, J.; Hu, Y. Optimized active power dispatching strategy considering fatigue load of wind turbines during de-loading operation. *IEEE Access* **2019**, *7*, 17439–17449. [CrossRef]
4. Kim, H.; Singh, C.; Sprintson, A. Simulation and estimation of reliability in a wind farm considering the wake effect. *IEEE Trans. Sustain. Energy* **2012**, *3*, 274–282. [CrossRef]
5. Hou, P.; Hu, W.; Soltani, M.; Chen, C.; Zhang, B.; Chen, Z. Offshore wind farm layout design considering optimized power dispatch strategy. *IEEE Trans. Sustain. Energy* **2016**, *8*, 638–647. [CrossRef]
6. Ma, Z.; Wang, D.; Zhang, H.; Wang, Y.; Dong, H. Two-stage optimal dispatching based on wind-photovoltaic-pumped storage-thermal power combined power generation system. In Proceedings of the 2019 IEEE 3rd Conference on Energy Internet and Energy System Integration (EI2), Changsha, China, 8–10 November 2019.
7. Al Shereiqi, A.; Al-Hinai, A.; Al-Abri, R.; Albadi, M. The effect of wind farm micro-siting on output power: A case study in Oman. In Proceedings of the 2020 6th IEEE International Energy Conference (ENERGYCon), Gammarth, Tunisia, 28 September–1 October 2020.
8. Ma, Y.; Yang, H.; Zhou, X.; Li, J.; Wen, H. The dynamic modeling of wind farms considering wake effects and its optimal distribution. In Proceedings of the 2009 World Non-Grid-Connected Wind Power and Energy Conference, Nanjing, China, 24–26 September 2009.
9. Li, M.; Qiu, Y.; Wang, X.; Feng, Y.; Cai, X.; Zhang, Z. Multi-Body Dynamic Modeling of Offshore Wind Turbine under Wake Effects. In Proceedings of the 10th Renewable Power Generation Conference, Virtual, 14–15 October 2021.
10. Zhang, B.; Soltani, M.; Hu, W.; Hou, P.; Huang, Q.; Chen, Z. Optimized power dispatch in wind farms for power maximizing considering fatigue loads. *IEEE Trans. Sustain. Energy* **2017**, *9*, 862–871. [CrossRef]
11. Charles, M.; Oyedokun, D.T.O.; Dlodlo, M. Wind Farm Density Effects on Turbulence Intensity for Large Hexagonal Farm Arrays. In Proceedings of the 2020 6th IEEE International Energy Conference (ENERGYCon), Gammarth, Tunisia, 28 September–1 October 2020.
12. Xu, R.; Zhang, G.; Zhang, K. Coordinated Control of Wind Farm Power Prediction Based on PSO-MPC Model. In Proceedings of the 2021 IEEE 2nd International Conference on Information Technology, Big Data and Artificial Intelligence (ICIBA), Chongqing, China, 17–19 December 2021.
13. Navya, V.; Ramesh, S.; Vijayapriya, R.; Raja, P. Optimization of Wind Farm Layout Based on Wake Effect Modelling. In Proceedings of the 2020 IEEE International Students' Conference on Electrical, Electronics and Computer Science (SCEECS), Bhopal, India, 22–23 February 2020.
14. Tian, J.; Su, C.; Soltani, M.; Chen, Z. Active power dispatch method for a wind farm central controller considering wake effect. In Proceedings of the IECON 2014–40th Annual Conference of the IEEE Industrial Electronics Society, Dallas, TX, USA, 29 October–1 November 2014.
15. Zhao, R.; Shen, W.Z.; Knudsen, T.; Bak, T. Fatigue distribution optimization for offshore wind farms using intelligent agent control. *Wind. Energy* **2012**, *15*, 927–944. [CrossRef]
16. Yang, J.; Zheng, S.; Song, D.; Su, M.; Yang, X.; Joo, Y.H. Comprehensive optimization for fatigue loads of wind turbines in complex-terrain wind farms. *IEEE Trans. Sustain. Energy* **2020**, *12*, 909–919. [CrossRef]
17. Sheng, J.; Chen, S. Fatigue load simulation for foundation design of offshore wind turbines due to combined wind and wave loading. In Proceedings of the 2010 World Non-Grid-Connected Wind Power and Energy Conference, Nanjing, China, 5–7 November 2010.
18. Lin, K.; Tang, X.-Y.; Zhao, W.; Ling, Z. Optimized Power Dispatch for Regional Fatigue Balancing in Offshore Wind Farms. In Proceedings of the 2021 China Automation Congress (CAC), Beijing, China, 22–24 October 2021.
19. Liu, J.; Liu, Y.; Zeng, D.; Liu, J.; Lü, Y.; Hu, Y. Optimal short-term load dispatch strategy in wind farm. *Sci. China Technol. Sci.* **2012**, *55*, 1140–1145. [CrossRef]
20. Solomin, E.; Hou, T.; Ma, X.; Sun, Y. Design and Optimization of Power Harvesting and Distribution for Offshore Wind Farms Using Semi-Physical Simulation. In Proceedings of the 2020 International Ural Conference on Electrical Power Engineering (UralCon), Chelyabinsk, Russia, 22–24 September 2020.
21. Zhao, H.; Wu, Q.; Huang, S.; Shahidehpour, M.; Guo, Q.; Sun, H. Fatigue load sensitivity-based optimal active power dispatch for wind farms. *IEEE Trans. Sustain. Energy* **2017**, *8*, 1247–1259. [CrossRef]
22. Pynaert, N.; Haas, T.; Wauters, J.; Crevecoeur, G.; Degroote, J. Wing Deformation of an Airborne Wind Energy System in Crosswind Flight Using High-Fidelity Fluid–Structure Interaction. *Energies* **2023**, *16*, 602. [CrossRef]
23. Campagnolo, F.; Schreiber, J.; Bottasso, C.L. Wake deflection control with wind direction changes: Wind tunnel comparison of different wind farm flow models. In Proceedings of the 2020 American Control Conference (ACC), Denver, CO, USA, 1–3 July 2020.

24. Sonoda, T.; Nakata, M. Multiple Classifiers-Assisted Evolutionary Algorithm Based on Decomposition for High-Dimensional Multiobjective Problems. *IEEE Trans. Evol. Comput.* **2022**, *26*, 1581–1595. [CrossRef]
25. Liang, H.; Zuo, L.; Li, J.; Li, B.; He, Y.; Huang, Q. A wind turbine control method based on Jensen model. In Proceedings of the 2016 International Conference on Smart Grid and Clean Energy Technologies (ICSGCE), Chengdu, China, 19–22 October 2016.
26. Wang, J.; Duan, B.; Su, Y.X. Optimization of active power output in offshore wind farms based on wake effect. *Autom. Electr. Power Syst.* **2015**, *39*, 26–32.
27. Zeng, L.; Wang, F.; Liu, D. Research on wind turbine wake model and overlapping in wind farm. In *Zhongguo Dianji Gongcheng Xuebao*; Chinese Society for Electrical Engineering: Beijing, China, 2011.
28. Lu, J.; Tao, T.; Yan, J.; Liu, Y. Pre-Calculation of Wind Turbine Blade Fatigue Damage by Machine Learning. In Proceedings of the 10th Renewable Power Generation Conference (RPG 2021), Online Conference, 14–15 October 2021.
29. Dobesch, H.; Kury, G.; Kury, G. *Basic Meteorological Concepts and Recommendations for the Exploitation of Wind Energy in the Atmospheric Boundary Layer: Österreichische Beiträge zu Meteorologie und Geophysik*; Zentralanst. für Meteorologie u. Geodynamik: Wien, Austria, 2006.
30. Mousavi, Y.; Bevan, G.; Kucukdemiral, I.B.; Fekih, A. Sliding mode control of wind energy conversion systems: Trends and applications. *Renew. Sustain. Energy Rev.* **2022**, *167*, 112734. [CrossRef]
31. Li, H.; Shi, K.; McLaren, P. Neural-network-based sensorless maximum wind energy capture with compensated power coefficient. *IEEE Trans. Ind. Appl.* **2005**, *41*, 1548–1556. [CrossRef]
32. Scolaro, M.; Kittner, N. Optimizing hybrid offshore wind farms for cost-competitive hydrogen production in Germany. *Int. J. Hydrogen Energy* **2022**, *47*, 6478–6493. [CrossRef]
33. Li, M.; Jiang, X.; Carroll, J.; Negenborn, R.R. A multi-objective maintenance strategy optimization framework for offshore wind farms considering uncertainty. *Appl. Energy* **2022**, *321*, 119284. [CrossRef]
34. Li, Y.Z.; Li, M.S.; Wen, B.J.; Wu, Q.H. Power system dispatch with wind power integrated using mean-variance model and group search optimizer. In Proceedings of the 2014 IEEE PES general meeting | conference & exposition, National Harbor, MD, USA, 27–31 July 2014.
35. Wang, Y.; Wang, L.; Song, S.; Wei, S.; Ren, Z. Active Power Allocation in Offshore Wind Power Frequency Modulation Mode with the Fastest Action Time Constraint. In Proceedings of the 2021 4th International Conference on Energy, Electrical and Power Engineering (CEEPE), Chongqing, China, 23–25 April 2021.
36. El-Khoury, C.N.; Kanaan, H.Y.; Mougharbel, I.; Al-Haddad, K. Implementation of a Series Z-source Very Sparse Matrix Converter in a PMSG-based WECS. In Proceedings of the 2018 IEEE International Conference on Industrial Technology (ICIT), Lyon, France, 20–22 February 2018.
37. Wang, S.; Yang, L. Variable coefficient droop control strategy for optimal participation of wind farm in primary frequency regulation considering wake superposition effect. In Proceedings of the 2021 4th International Conference on Energy, Electrical and Power Engineering (CEEPE), Chongqing, China, 23–25 April 2021.
38. Ding, H.; Hu, Z.; Song, Y. Rolling optimization of wind farm and energy storage system in electricity markets. *IEEE Trans. Power Syst.* **2014**, *30*, 2676–2684. [CrossRef]
39. Zhang, B.; Xu, G.; Zhang, Z. A holistic robust method for optimizing multi-timescale operations of a wind farm with energy storages. *J. Clean. Prod.* **2022**, *356*, 131793.
40. Wang, J.; Li, D.; Lv, X.; Meng, X.; Zhang, J.; Ma, T.; Pei, W.; Xiao, H. Two-Stage Energy Management Strategies of Sustainable Wind-PV-Hydrogen-Storage Microgrid Based on Receding Horizon Optimization. *Energies* **2022**, *15*, 2861. [CrossRef]